Journal of the European Ceramic Society 23 (2003) 229–241

www.elsevier.com/locate/jeurceramsoc

Sintering of calcium phosphate hydroxyapatite $Ca_{10}(PO_4)_6(OH)_2$ I. Calcination and particle growth

D. Bernache-Assollant[a,*], A. Ababou[a], E. Champion[a], M. Heughebaert[b]

[a]*Science des Procédés Céramiques et de Traitements de Surface, UMR CNRS 6638, 123 avenue Albert Thomas, 87060 Limoges Cedex, France*

[b]*CIRIMAT, UMR CNRS 5085, 38, rue des 36 ponts, 31400 Toulouse, France*

Received 12 February 2002; received in revised form 15 May 2002; accepted 25 May 2002

Abstract

The influence of the temperature and the partial pressure of water vapour on the kinetic of surface reduction of hydroxyapatite during calcination treatment was studied. The water vapour catalysed the growth of HAP grains. A theoretical model was proposed and compared with the experimental data. It allowed the identification of the mechanisms of surface reduction and the determination of the kinetic laws. At low temperature ($T < 850\ ^\circ C$), grain coalescence occurs without densification. The superficial diffusion is the predominant mechanism and it is controlled by the adsorption–desorption of water vapour on the surface of the HAP grains. At higher temperature, the densification mechanisms are effective.

Keywords: Apatite; Calcination; Grain growth; Diffusion; Sintering

1. Introduction

Calcium phosphate hydroxyapatite $Ca_{10}(PO_4)_6(OH)_2$ (HAP) is commonly used as a bioceramic either in the form of dense sintered parts or of powder.[1–3] Numerous works have been devoted to the shaping and densification of HAP parts or to the elaboration of coatings and to their physico-chemical and biological characterisations.[4–15] But, very few studies have investigated the sintering mechanisms of this ceramic so that its behaviour remains misinterpreted.[16–18] But, the understanding of sintering is of prime importance because this allows the identification of the influent parameters and therefore to control the grain growth and the microstructural design of the ceramics. From these bases, the present study is concerned with a fundamental approach of the sintering of HAP, from the calcination of powders to the densification of ceramic materials.

The calcination constitutes a necessary step of the preparation when wet chemical routes are used for the synthesis of HAP, i.e. precipitation from the neutralisation of $Ca(OH)_2$ with H_3PO_4 or from the decomposition of $Ca(NO_3)_2$ and $(NH_4)_2HPO_4$.[19,20] Moreover, the analysis of particle growth during calcination is required for the understanding of grain growth phenomena that occur during the final stages of the densification.

This paper is the first part of a two-part work. It deals with the particle growth during the calcination of powders, analysed through the reduction of surface area of powders. The second part will concern the densification of HAP ceramics either by natural sintering or by hot pressing.

The temperature and the atmosphere of treatment are the most important parameters responsible for the surface reduction of ceramic powders.[21] Concerning the atmosphere, the water vapour is known to affect the behaviour of numerous oxides and hydroxides.[22–26] HAP may partially dehydrate to form oxyhydroxyapatite $Ca_{10}(PO_4)_6(OH)_{2-x}O_x$ and decompose into tricalcium phosphate $Ca_3(PO_4)_2$ and tetracalcium phosphate $Ca_4(PO_4)_2O$ at temperatures that depend on the atmosphere.[27] Consequently, the influence of both the temperature and the partial pressure of water vapour on the kinetic of surface reduction of HAP powders have been investigated. A theoretical model

* Corresponding author. Tel.: +(0)5-5545-7370; fax: +(0)5-5545-7586.

E-mail address: bernache@unilim.fr (D. Bernache-Assollant).

0955-2219/02/$ - see front matter © 2002 Elsevier Science Ltd. All rights reserved.
PII: S0955-2219(02)00186-3

based on the elementary steps of the process of surface area reduction is proposed and compared with the experimental data.

2. Experimental procedures

2.1. Powder preparation

Hydroxyapatite powder was precipitated in an aqueous medium by slow addition of a diammonium phosphate solution containing NH_4OH into a boiling calcium nitrate $Ca(NO_3)_2{,}4H_2O$ solution, also containing NH_4OH, under constant stirring. The pH of the mixture was about 9. After total addition of the reactants the suspension was filtered without washing and dried at 80 °C for 12 h. The powder was disagglomerated by light grinding in the presence of ethanol. The Ca/P molar ratio, determined using a standardised X-ray diffractometry method with CuK_α radiation (Siemens D5000 apparatus, Germany) on the powder heated at 1000 °C, was 1.667.[28,29] Only HAP peaks were detected as shown on the X-ray diffraction (XRD) pattern (Fig. 1).

2.2. Calcination

Calcination treatments of the powder were carried out in a horizontal furnace with an alumina tube. They were performed in air or in oxygen atmosphere containing a controlled partial pressure of water vapour (P_{H_2O}). This partial pressure of H_2O was fixed by the temperature of a thermostatic bath and the water vapour was conveyed through the alumina tube using the oxygen as vector. The horizontal furnace was fed with water vapour, and then the HAP sample was introduced. The calcinations were not conducted under strict isothermal conditions; the isothermal temperatures were reached at the heating rate of 25 °C/min. This high rate allows to proceed close to isothermal conditions but the initial time, that is to say the moment at which a sample reaches the isothermal temperature remains imprecise. This could make difficult any interpretation for very short times. The samples were removed from the furnace after having been kept at constant temperature for various times, then their specific surface area was measured.

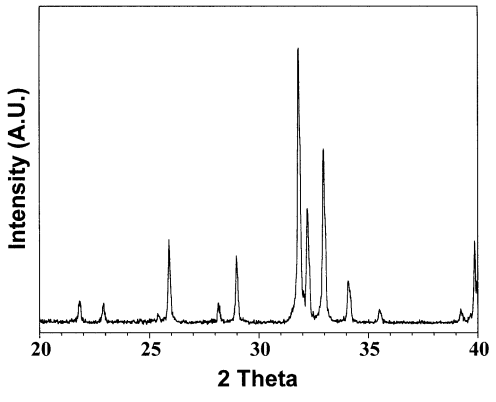

Fig. 1. XRD pattern of HAP powder calcined at 1000 °C.

2.3. Densification

The linear shrinkage of HAP was determined by dilatometry (Setaram TMA 92, France) on cylindrical samples. The samples were heated in air up to the temperature of 1250 °C at a heating rate of 5 °C/min. The samples (about 0.5 g) were initially pressed under a 150 MPa compressive stress in a cylindrical die (diameter = 10 mm). The density of the fired samples was determined after polishing by weighing and geometrical measurements of the specimens. The densification ratio was calculated assuming a theoretical density of 3.156 for the HAP.

2.4. Characterization

The specific surface area was measured by the BET method using nitrogen adsorption at 77 K (analyzer Micromeritics 2205, USA) with the single point method after degasing the powder at 350 °C under argon. Each point is the average of three measured values. An estimated value for the dried powder was 60 m^2/g.

Agglomerate size and grain size distributions of the powder were performed using an X-ray granulometer (Micromeritics Sedigraph 5000, USA). In the first case, the powder was not disagglomerated before measurement. In the second case, the powder was ultrasonically dispersed before measurement in order to break the agglomerates. The values of both agglomerate size and grain size were confirmed by observation using scanning electron microscopy (SEM, Hitachi S2500, Japan). The size of the elementary crystallites was calculated using the Scherrer formula from the half width of the diffraction peak of HAP at $2\theta = 40°$.

3. Results

The sintering theories indicate that the reduction of the surface area of a powder can result from different mechanisms of matter transport that can be divided in two categories. Superficial diffusion and gaseous phase transport lead generally to a reduction of surface area without densification of the material. In contrast, volume diffusion or grain boundaries diffusion induces a reduction of surface accompanied with an increase of the apparent density. Thus, the study of the densification of powders in relation with the surface changes allows the identification of the category of the matter transport responsible for the surface reduction. To this

end, a dilatometric study was first performed to determine the temperature at which the densification of the material begins.

3.1. Densification

Fig. 2 shows the linear shrinkage of HAP versus the temperature. The densification began at about 850 °C. As pointed out on the derivative plot of linear shrinkage, the curve presented an inflexion at 1100 °C that corresponded to the maximum rate of densification. After cooling to room temperature, the densification ratio of the sample was 96% of the theoretical density.

From these results it can be deduced that below 850 °C, a decrease of the specific surface area must be attributed to mechanisms of matter transport occurring without densification, i.e. superficial diffusion or gaseous phase transport. Above 850 °C, mechanisms that densify, i.e. volume or grain boundary diffusion, must be taken in account of.

3.2. Surface area reduction

3.2.1. Influence of the heating atmosphere

The use of oxygen as an inert carrier gas of water vapour required that the pressure of oxygen did not influence the reduction of surface area of HAP powders. This was verified by calcining the powders at 860 °C during 1 h under pure oxygen at different pressures varying between 20 and 103 kPa. The surface area remained constant whatever the oxygen pressure might be (Fig. 3).

The changes of specific surface area of powders calcined for 1 h in the 500–1000 °C temperature range in air, pure oxygen and 14.5 kPa of water vapour in oxygen are given in Fig. 4. The plots showed that the surface decrease was more important in the presence of vapour water, pointing out its catalytic effect on the surface reduction of HAP. This influence was confirmed from the evolution of the surface area of powders calcined at 860 °C for 1 h in different partial pressures of water vapour (Fig. 5). The surface decrease was more and more important as P_{H_2O} increased. Nevertheless, a threshold seemed reached for partial pressures above 15 kPa. Typical SEM micrographs of powders heated in these different atmospheres are given in Fig. 6. Compared with the as synthesized powder evidence exists for a particle coalescence associated with the surface reduction.

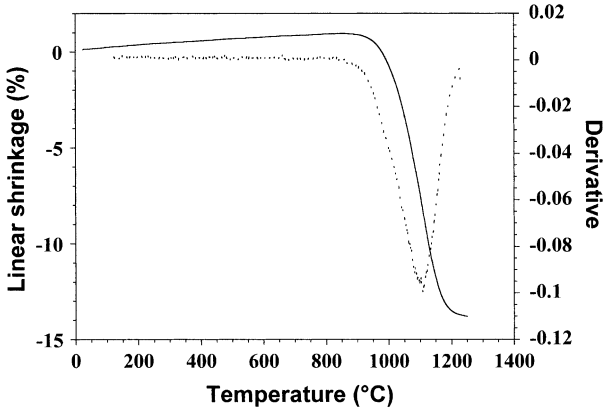

Fig. 2. Linear shrinkage of HAP versus the temperature (heating rate 5 °C/min) and derivative plot (dashed line).

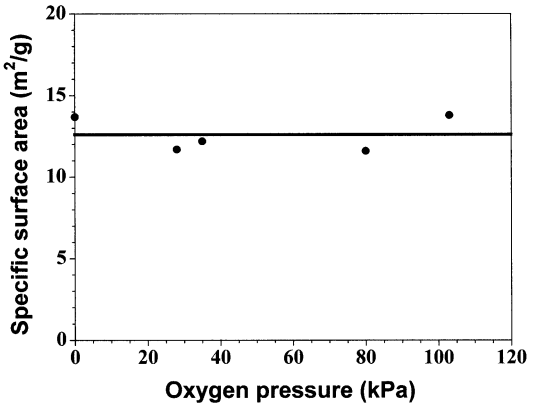

Fig. 3. Specific surface area of HAP powders after calcination in pure oxygen at 860 °C during 1 h.

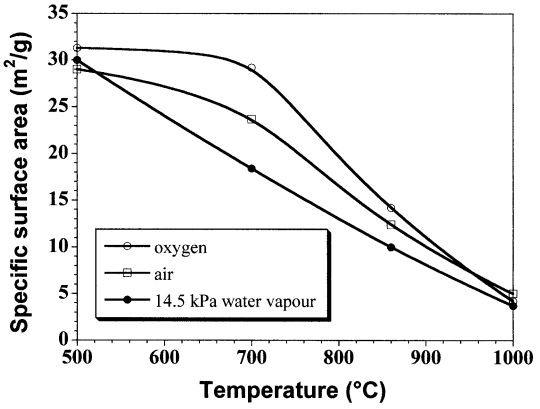

Fig. 4. Specific surface area of HAP powders after calcination for 1 h in different atmospheres versus the calcination temperature.

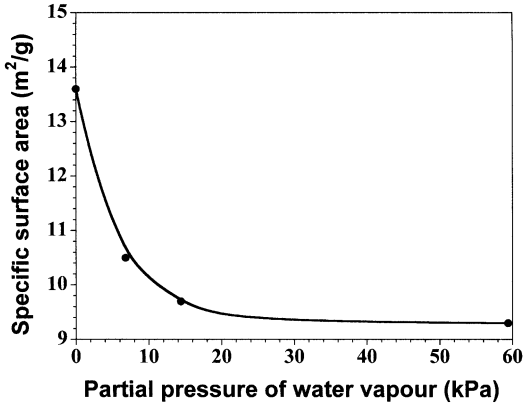

Fig. 5. Specific surface area of HAP powders after calcination in oxygen containing water vapour at 860 °C during 1 h.

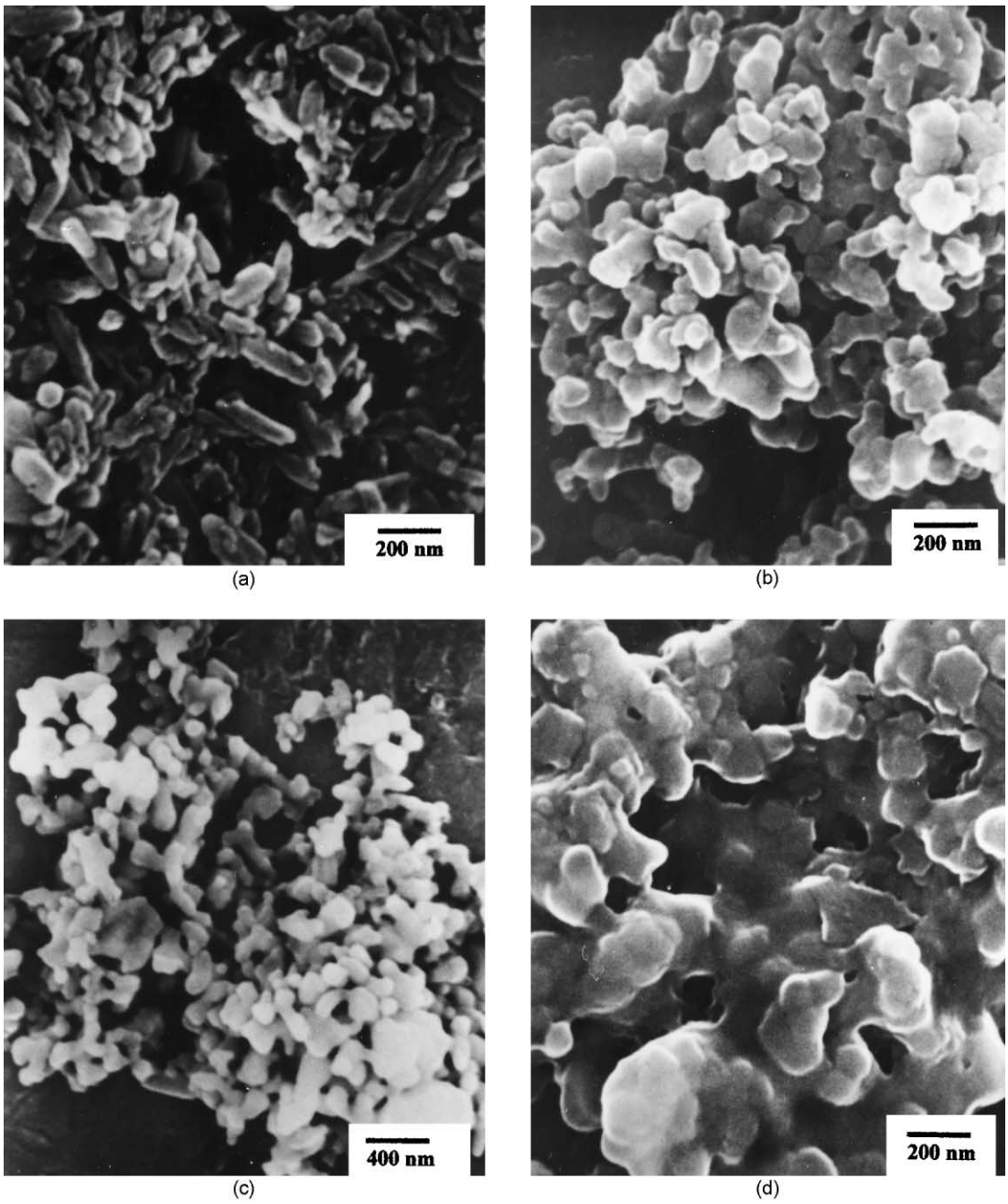

Fig. 6. SEM micrographs of HAP powder after calcination treatment at 860 °C for 1 h: (a) as synthesized; (b) calcined in pure oxygen; (c) calcined in air; (d) calcined in oxygen containing 59.4 kPa of water vapour.

From this first approach, it can be concluded that pure oxygen can be used as a carrier gas for water vapour and that the reduction of surface area of HAP powders is strongly dependent on the partial pressure of water vapour. These results have also shown that the densification began at about 850 °C. Consequently, the surface reduction has to be investigated in the two domains of temperature, above and below the beginning of the densification. It must be characterized either under isothermal conditions in order to precise the influence of the partial pressure of water vapour or under isobar conditions to determine the influence of the temperature.

3.2.2. *Influence of the partial pressure of water vapour*

The temperature of 860 °C was chosen for the experiments in the domain of high temperatures ($T > 850$ °C). The powder samples were removed from the furnace after having been kept at 860 °C for various times, then their specific surface area was measured (Fig. 7). It can be noted that the diminution of the surface was more important during the first minutes of

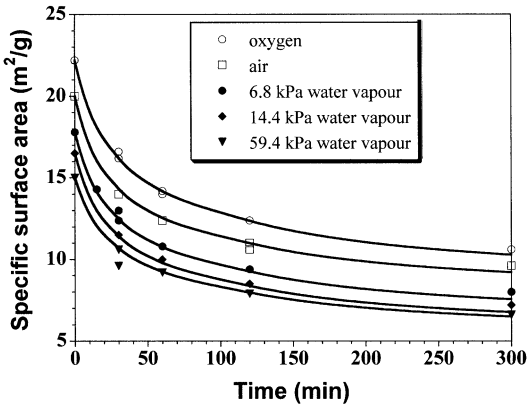

Fig. 7. Specific surface area of HAP powders after calcination in different atmospheres versus the calcination time. Line drawings represent Eq. (1).

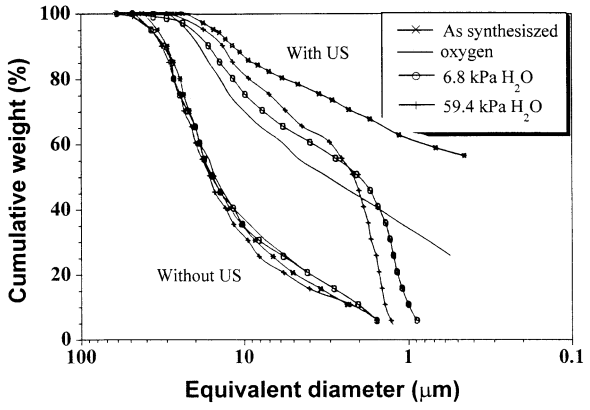

Fig. 8. Agglomerate size (without ultrasonic dispersion) and grain size (with us dispersion) distributions of powders calcined at 860 °C for 1 h in different atmospheres.

calcination and that the augmentation of P_{H_2O} increased the surface reduction. The dots on Fig. 7 are experimental data and line drawings correspond to the following equation fitted to the experimental data:

$$S = S_0(1 + At)^p \quad (1)$$

where S is the surface area at a time t, S_0 is the initial surface area and A and p are determined by the fitting procedure. The fitted values of A and p are summarised in Table 1.

The agglomerate size and grain size distributions of powders after calcination at 860 °C for 1 h in different atmospheres are given in Fig. 8. The plots can be divided in two groups. Without ultrasonic dispersion, no change was observed in the agglomerate size distributions whatever the atmosphere of treatment might be. In contrast, the distributions obtained after ultrasonic dispersion of the powders showed that the presence of water vapour induced a narrower grain size distribution shifted towards larger sizes. These results mean that the morphological modifications induced by the thermal treatments concern only the elementary grains inside the agglomerates. The shift observed with vapour water corresponds to a grain growth that can originate either in an Ostwald ripening or in a sintering of the smallest grains producing coarser ones. The crystallite size determined from XRD peaks showed few changes with the atmosphere of calcination (Fig. 9). Crystallite size

Table 1
Fitted values of A and p of Eq. (1) and calculated value of m using Eq. (4) for powders calcined at 860 °C in different atmospheres

Atmosphere	O_2	Air	H_2O (6.8 kPa)	H_2O (14.4 kPa)	H_2O (59.4 kPa)
A	0.127	0.158	0.135	0.133	0.123
p	−0.21	−0.20	−0.23	−0.24	−0.23
m	5.76	6	5.34	5.16	5.34

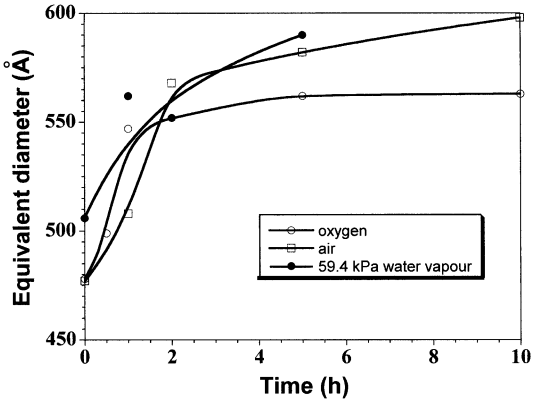

Fig. 9. Crystallite size (Scherrer method) of HAP powders versus the calcination time at 860 °C.

was about 50–60 nm, which was smaller than the grain size (Fig. 8). As a consequence, grains are not single crystals and it can be stated that the decrease of the surface area during the calcination should be due to grain coalescence rather than crystallites growth that could be attributed to grain boundaries migration.

Similar experiments were performed at 600 °C in the domain of low temperatures ($T < 850$ °C). The specific surface area of HAP powders calcined for various times in oxygen containing different partial pressures of water vapour is given in Fig. 10. As for the powders calcined at 860 °C, the plots show the catalytic effect of the water vapour on the surface reduction. The fitted values of A and p of Eq. (1) are presented in Table 2. It can be seen that the values of these fitted parameters differ considerably from those determined at 860 °C (Table 1), indicating that the mechanisms occurring at the two temperatures (600 and 860 °C) are different.

3.2.3. Influence of the temperature

The curves of surface area of powders calcined in the temperature range 300–900 °C under isobar conditions (6.8 kPa of water vapour) are shown in Fig. 11. The

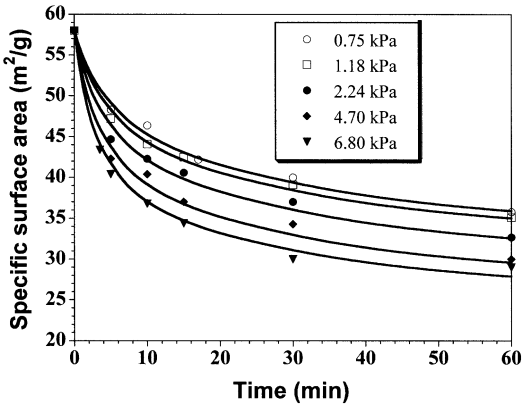

Fig. 10. Specific surface area of HAP powders after calcination at 600 °C in different partial pressures of water vapour versus the calcination time. Line drawings represent Eq. (1).

Table 2
Fitted values of A and p of Eq. (1) and calculated value of m using Eq. (4) for powders calcined at 600 °C in the presence of water vapour

P_{H_2O} (kPa)	0.75	1.18	2.24	4.70	6.80
A	0.496	0.596	0.76	1.1	1.6
p	−0.14	−0.14	−0.15	−0.16	−0.16
m	8.1	8.1	7.7	7.3	7.3

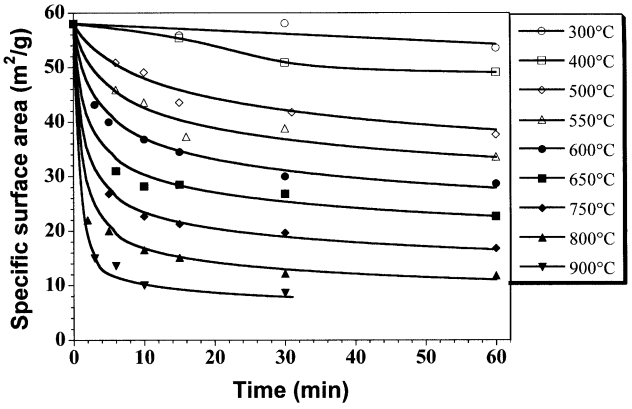

Fig. 11. Specific surface area of HAP powders after calcination at different temperatures in 6.8 kPa of water vapour versus the calcination time. Line drawings represent Eq. (1).

decrease of the surface area became noticeable from 500 °C. The main drop occurred at the beginning of the calcination isotherm (during the first 10 min). The values of A and p determined from the fittings of Eq. (1) to the experimental dots under these isobar conditions (Table 3) agree with those obtained from isothermal conditions (Tables 1 and 2). An important diminution of p values can be noted for high temperatures (about −0.16 at low temperature and −0.23 at high temperature). This change corresponds to the beginning of the densification and consequently to an expected change in the mechanisms of matter transport.

Table 3
Fitted values of A and p of Eq. (1) and calculated values of m using Eq. (4) for powders calcined at different temperatures for $P_{H_2O} = 6.8$ kPa

Temperature	500	550	600	650	750	800	900
A	0.29	0.82	1.6	5.8	12	22.3	191
p	−0.14	−0.14	−0.16	−0.16	−0.19	−0.23	−0.23
m	8.1	8.1	7.3	7.3	6.2	5.3	5.3

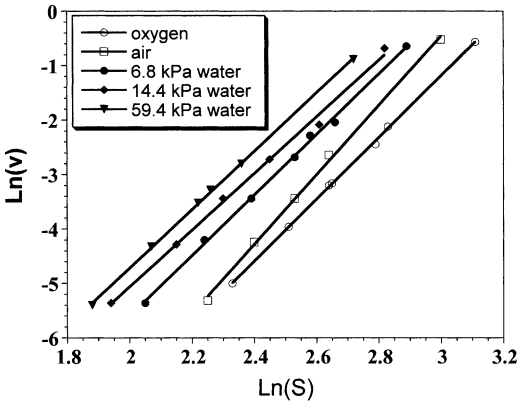

Fig. 12. Rate of surface reduction (Ln) versus the surface area (Ln) of powders calcined at 860 °C in different atmospheres.

4. Discussion

It is possible to determine the rate of surface reduction (dS/dt) either as a function of the pressure of water vapour for a constant value of the surface or as a function of the surface for a constant pressure of water vapour.

Fig. 12 gives the rate of surface area reduction versus the surface value for powders calcined at 860 °C in different atmospheres. The resulting linear plots in logarithm coordinates for each atmosphere show that the rate can be defined as follows:

$$v = \frac{dS}{dt} = k \times f(P_{H_2O}) \times S^{m} \quad (2)$$

where k is the rate constant, $f(P_{H2O})$ is a function of the partial pressure of water vapour and m is the surface exponent that is characteristic of the mechanism of matter transport.

The derivative of Eq. (1) used to describe the isothermal plots of surface area reduction leads to the rate of surface change $\frac{dS}{dt}$ and allows to link the parameters k and m of Eq. (2) to the values of A and p as:

$$k = p \times A \times S_0^{1/p} \quad (3)$$

$$m = (p-1)/p \quad (4)$$

The calculated values of m for the different atmospheres of calcination at 860 °C are given in Table 1. All

the values of m are close (between 5.34 and 6) indicating that the mechanism responsible for the surface drop is the same and does not depend on the composition of the gaseous atmosphere of calcination.

The influence of the pressure of the water vapour on the kinetic function $f(P_{H_2O})$ of Eq. (2) has been determined through the plots of the rate of surface reduction versus the pressure of water vapour for fixed values of surface area (Fig. 13). The linear plots obtained in logarithm coordinates indicate that the rate is such as:

$$v = \frac{dS}{dt} = k \times g(S) \times P^n_{H_2O} \quad (5)$$

where $g(S)$ is the function of the surface [defined in Eq. (2)] and n is the pressure exponent. In these experiments n was found between 0.27 and 0.28.

Finally, the rate of surface area reduction of HAP at 860 °C obeys the following kinetic law:

$$v = k \times P^n_{H_2O} \times S^m \quad (6)$$

In the same way, the linear plots of Ln(v) versus Ln(S) for different partial pressures of water vapour (Fig. 14) and the linear plots of Ln(v) versus Ln(P_{H_2O}) for different values of the surface (Fig. 15) allowed the establishment of a similar law of variation of the surface area [Eq. (6)] for powders calcined at 600 °C. The calculated values of m at 600 °C are given in Table 2. They are between 7.3 and 8.1. The pressure exponent was between 0.65 and 0.72 depending on the value of the surface area retained for the calculation. The average value of n is 0.68 and its variations in the investigated domain can be ascribed to the experimental discrepancies. These values of m and n are noticeably superior to those found at 860 °C, which confirms a change of mechanism between these two temperatures of 600 and 860 °C.

In the case of the isobar experiments with $P_{H_2O} = 6.8$ kPa, the kinetic law of surface area reduction also could be expressed by the Eq. (6). The associated values of the surface exponent m calculated using Eq. (4) are presented in Table 3. Constant values of m were found at the ends of the temperature range, i.e. 5.3 and 8.1 for high and low temperatures respectively, the values changing progressively between these extremes for intermediate temperatures. The kinetic constant k of Eq. (6) versus the temperature can be represented through an Arrhenius plot (Fig. 16). The plots could be divided in two different linear domains, each one being associated with an activation energy. The slopes of the linear regressions give an activation energy of 117 and of 208 kJ/mol in the domains of low and high temperatures, respectively.

A model of the reduction of surface area of a ceramic powder has been established by German et al.[30,31] It has been satisfactory applied to explain the origins of matter transports in very different compounds such as magnesium oxide or uranium dioxide. Nevertheless, the laws of surface area reduction have been validated only in the case of a relative variation of the surface of less than 50%, which does not correspond to our experiments on the HAP powder, the surface area varying from about 60 m^2/g down to about 1 m^2/g. Other models have been proposed to describe the reduction of surface area of

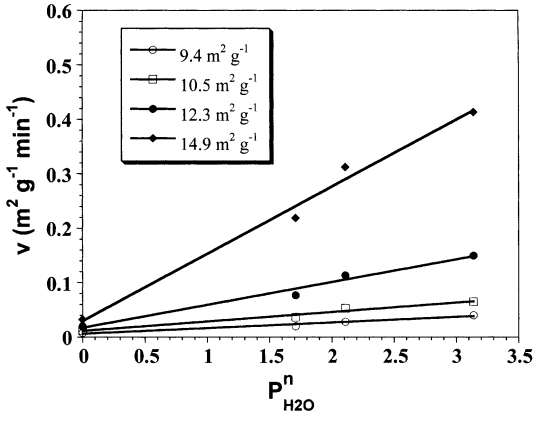

Fig. 13. Rate of surface reduction of powders calcined at 860 °C for fixed surface areas versus $P^n_{H_2O}$ with $n = 0.28$.

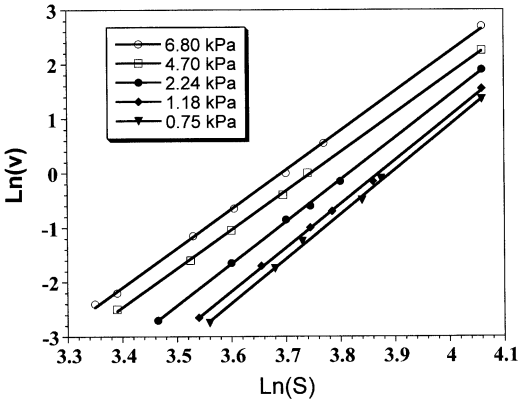

Fig. 14. Rate of surface reduction (Ln) versus the surface area (Ln) of powders calcined at 600 °C in different P_{H_2O}.

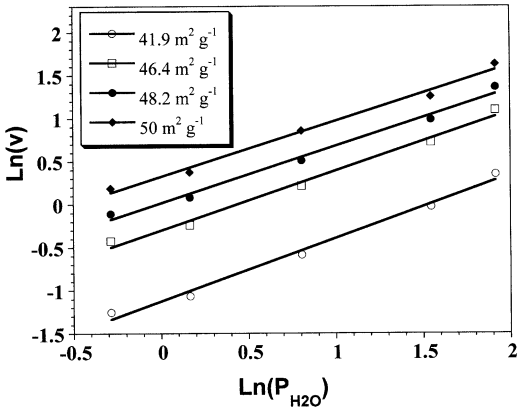

Fig. 15. Rate of surface reduction (Ln) of powders calcined at 600 °C for fixed surface ereas versus P_{H_2O} (Ln).

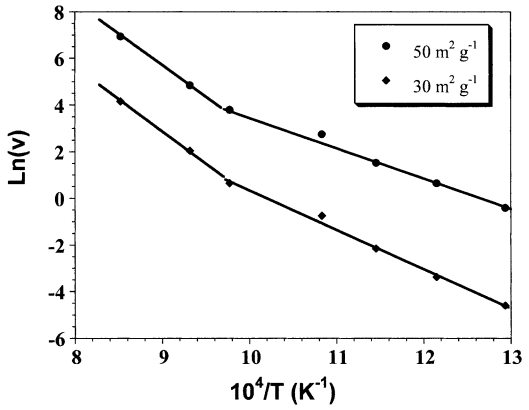

Fig. 16. Arrhenius plots of the surface reduction of HAP powders for $P_{H_2O} = 6.8$ kPa and fixed values of the specific surface area.

catalysts. Ruckenstein,[32] Hashimoto[33] and Gruy[34] give an expression of the reduction of surface area of catalysts particles dispersed on the surface of a solid that includes several successive steps: in a first step, the particles move closer to one another and necks develop between them, then in a second step particles coalescence occurs. The models integrate the size distribution of the particles and its time dependence. If the kinetic is controlled by the building of the necks, the law is:

$$\frac{dS}{dt} = k\ S^m$$

The theoretical values of the surface exponent m, summarized in Table 4, depend on the diffusion mechanism: m is equal to 8 for superficial diffusion and 6 for evaporation–condensation.

In the low temperature domain, the value of m (between 7.3 and 8) can be attributed to superficial diffusion. This mechanism agrees with the low activation energy found at 600 °C (117 kJ/mol). At high temperature the value of m (between 5.3 and 6) could correspond to a mechanism of evaporation–condensation.

5. Model for surface area reduction of HAP powder during the calcination in the presence of water vapour

Few models of surface area reduction take the partial pressure of the water vapour on account of. We propose to describe the grain growth of HAP powders by a model of particle coalescence in which the water vapour is considered as a catalyst. This approach is derived from the works of Hebrard et al. that described the surface area reduction of titania anatase powder in different atmospheres.[22]

Table 4
Theoretical values of the surface exponent m of the law $v = k\ S^m$, from Refs. 33 and 34

Mechanism	m
Surface diffusion	8
Gaseous phase transport	7
Evaporation-condensation	6
Surface reaction	5

5.1. Thermodynamic equilibrium between HAP and the water vapour

At first, we have considered the equilibrium of dehydration of the HAP into oxyhydroxyapatite:

$$Ca_{10}(PO_4)_6(OH)_2 = Ca_{10}(PO_4)_6(OH)_{2-2x}O_x + x\ H_2O$$

This reaction induces the creation of hydroxide vacancies (noted V^o_{OH}) and oxygen ions O^{2-} (noted O'_{OH}) that replace the hydroxide ions OH^- (noted OH^x_{OH}). Using these structural elements the dehydration equilibrium can be written as:

$$2\ OH^x_{OH} = O'_{OH} + V^o_{OH} + H_2O$$

The constant of this equilibrium will be noted K_1. Though OH^x_{OH} is a structural element of the HAP network its molar ratio can't be considered as equal to 1 because of possible important variations of the stoichiometry during the dehydration. Therefore, in these hydroxide sites the molar fractions of oxygen ions ($X_{O'_{OH}}$), of hydroxide vacancies ($X_{V^o_{OH}}$) and of hydroxide ions ($X_{OH^x_{OH}}$) relate as follows:

$$X_{V^o_{OH}} = X_{O'_{OH}}$$

and

$$X_{V^o_{OH}} + X_{O'_{OH}} + X_{OH^x_{OH}} = 1$$

Consequently:

$$X_{V^o_{OH}} = \frac{1 - X_{OH^x_{OH}}}{2}$$

On the assumption that the solution between the occupied and free hydroxide sites behaves ideally, the molar fractions are equal to the activities. They can be defined versus the equilibrium constant K_1 and the pressure of water vapour as:

$$X_{V^o_{OH}} = \frac{K_1^{\frac{1}{2}}}{2K_1^{1/2} + P^{1/2}_{H_2O}}$$

and

$$X_{OH^x_{OH}} = \frac{P^{1/2}_{H_2O}}{2K_1^{1/2} + P^{1/2}_{H_2O}}$$

These molar fractions correspond to the equilibrium of HAP with the gaseous atmosphere in which thermodynamic and kinetic effects of grains curvature has been neglected.

If we suppose that hydroxyapatite may exist in a gaseous state with its molecular formula $Ca_{10}(PO_4)_6(OH)_2$, it is possible to define the influence of the pressure of water vapour on the sublimation equilibrium:

$$Ca_{10}(PO_4)_6(OH)_{2(solid)} = Ca_{10}(PO_4)_6(OH)_{2(gas)}$$

The constant of this equilibrium will be noted K_s.

From a thermodynamic point of view, oxyhydroxyapatite $Ca_{10}(PO_4)_6(OH)_{2-2x}O_x$ can be considered as a solid solution of $(1-x)$ mol of hydroxyapatite $Ca_{10}(PO_4)_6(OH)_2$ and x mol of oxyapatite $Ca_{10}(PO_4)_6O$:

$$Ca_{10}(PO_4)_6(OH)_{2-x}O_x = (1-x)\ Ca_{10}(PO_4)_6(OH)_2 + x Ca_{10}(PO_4)_6O$$

If P_{HA} is the partial pressure of HAP and X_{HA} the molar fraction of HAP in this solid solution, the equilibrium constant of sublimation K_s can be written as:

$$K_s = \frac{P_{HA}}{X_{HA}}$$

with

$$X_{HA} = 1-x$$

and

$$X_{HA} = X_{OH^x_{OH}}$$

Finally the partial pressure of HAP in the gaseous phase can be expressed as:

$$P_{HA} = K_s \times \frac{P_{H_2O}^{1/2}}{2K_1^{1/2} + P_{H_2O}^{1/2}}$$

According to this last expression, the partial pressure of sublimation should be independent of P_{H_2O} for high partial pressures of water vapour and proportional to $P_{H_2O}^{1/2}$ for low pressures of water vapour.

5.2. Hydroxyapatite grain growth

5.2.1. Grain growth by surface diffusion

The grain growth of HAP powders by superficial diffusion is described on the same basis as the model developed by Hebrard for the interpretation of titania grain growth under water vapour.[22]

The process of grain growth can be described by the transport of HAP molecules from the surface of a grain with a positive curvature ($r>0$) towards the surface of a neck with a negative curvature ($r<0$). This transport can be divided in seven elementary steps:

(I) Dehydration of the surface:

$$2\left(OH^x_{OH}\right)_{r>0} = \left(O'_{OH}\right)_{r>0} + \left(V^o_{OH}\right)_{r>0} + H_2O \qquad (I)$$

(II) Diffusion of a superficial defect O'_{OH} from a positive curvature surface towards a negative curvature surface:

$$\left(O'_{OH}\right)_{r>0} + \left(V^o_{OH}\right)_{r<0} \rightarrow \left(O'_{OH}\right)_{r<0} + \left(V^o_{OH}\right)_{r>0} \qquad (II)$$

(III) Building of a structural unit of HAP on the surface of the neck by coalescence of oxygen defects:

$$2\left(O'_{OH}\right)_{r<0} + 2\left(O'_{OH}\right)_{r<0} = 4\left(O'_{OH}\right)_{r<0} + 10\left(V''_{Ca}\right)_{r<0} + 6\left(V^{ooo}_{PO_4}\right)_{r<0} + 2\left(V^o_{OH}\right)_{r<0} \qquad (III)$$

(IV) Fixation of water on the surface of the neck

$$H_2O + \left(V^o_{OH}\right)_{r<0} + \left(O'_{OH}\right)_{r<0} = 2\left(OH^x_{OH}\right)_{r<0} \qquad (IV)$$

(V) Diffusion of PO_4^{3-} ions through vacancies from the surface of the grain towards the surface of the neck:

$$\left(PO^x_{4_{PO_4}}\right)_{r>0} + \left(V^{ooo}_{PO_4}\right)_{r<0} \rightarrow \left(PO^x_{4PO_4}\right)_{r<0} + \left(V^{ooo}_{PO_4}\right)_{r>0} \qquad (V)$$

(VI) Diffusion of Ca^{2+} ions from the surface of the grain towards the surface of the neck:

$$\left(Ca^x_{Ca}\right)_{r>0}\left(V''_{Ca}\right)_{r<0} \rightarrow \left(Ca^x_{Ca}\right)_{r<0} + \left(V''_{Ca}\right)_{r>0} \qquad (VI)$$

(VII) Annihilation of vacancies on the surface of the neck:

$$10\left(V''_{Ca}\right)_{r>0} + 6\left(V^{ooo}_{PO_4}\right)_{r>0} + 2\left(V^o_{OH}\right)_{r>0} = 0 \qquad (VII)$$

For the concentrations of the different species, the following notations will be used:

$$\left[V''_{Ca}\right] = c \quad \left[V^{ooo}_{PO_4}\right] = a \quad \left[O'_{OH}\right] = o \quad \left[V^o_{OH}\right] = h \quad \left[OH^x_{OH}\right] = O$$

These species can exist either in the volume or on the surface of the HAP grains. If the specie is on the surface, the sign of the curvature will be added in subscript,

for example c_+ ($r>0$) or c_- ($r<0$). Moreover, if the values correspond to the equilibrium concentrations the letter e will be added in subscript.

The constants of the equilibrium of the steps (I), (III), (IV) and (VII) supposed at the equilibrium state can be written as follows:

$$K_1 = \frac{h_{+e}.o_{+e}.P_{H_2O}}{O^2_{+e}}$$

$$K_3 = h^2_{-e}.a^6_{-e}.c^{10}_{-e}$$

$$K_4 = \frac{O^2_{-e}}{h_{-e}.o_{-e}.P_{H_2O}}$$

$$K_7 = \frac{1}{c^{10}_{+e}.a^6_{+e}.h^2_{+e}}$$

When the steady state is reached, the concentrations of the different species are constant and their derivative is equal to zero, which leads to the following relations between the rates v_i of the elementary steps i:

$$v_1 = v_2 = v_3 = v_4 = v_7 = \frac{v_5}{6} = \frac{v_6}{10}$$

The electroneutrality gives the relation:

$$3a + h = 2c + o$$

On the logical assumption that the defects V^{o}_{OH} and O'_{OH} are a majority, the electroneutrality becomes:

$$h = o$$

If the initial hydroxyapatite verifies the calcium and phosphorus stoichiometry, then:

$$5a = 3c$$

As for the thermodynamic approach, the hydroxide sites must verify:

$$o + O + h = 1$$

The sintering rate can be identified with v_7, because the step (VII) is associated with the disappearance of a structural unit of HAP of the surface of a grain. The limiting step imposes its rate to the whole process of grain growth. This means that the other steps have infinite rate constants k_i and k_i' (for the direct and reverse reaction, respectively) but their ratio k_i/k_i' is finite. We have assumed that the proposed steps are associated with elementary reactions and that the slowest step is far from the equilibrium. In this case, the stoichiometric coefficients of the reactions are the partial orders of the kinetic law and the single direct reactions can be used. On these bases, we have established the rate law of each step in considering it as the limiting one. The main hypotheses and calculations are detailed hereafter for the steps (I) and (II), which correspond to a reactional and diffusional kinetic, respectively.

•*Step (I): kinetic of pure dehydration*. If the reverse reaction is neglected, the rate is given by:

$$v_1 = k_1.O^2_+$$

The rate of superficial diffusion being fast, the following relations are verified:

$$o_+ = o_- \quad a_+ = a_- \quad h_+ = h_- \quad O_+ = O_-$$

The superficial electroneutrality (admitted hypothesis) implies that $o = h$. The values of these concentrations will be set equal to those of the surface of the grain, the surface of a neck being much smaller. Thus: $o_+ = h_+$.

The superficial concentration and the molar fraction of a structural element are proportional. Consequently, the equilibrium constants that relate to the molar fractions will be used also for the concentrations. From the previous relations, the hydroxide concentration can be deduced as:

$$O = \frac{K_4^{1/2}.P^{1/2}_{H_2O}}{2 + K_4^{1/2}.P^{1/2}_{H_2O}}$$

This corresponds to a rate v_1 such as:

$$v_1 = k_1 \frac{K_4.P_{H_2O}}{(2 + K_4^{1/2}.P^{1/2}_{H_2O})^2}$$

For a low pressure of water vapour this rate is proportional to P_{H_2O} whereas for a high pressure it is independent of P_{H_2O}. For intermediate pressures, the rate could be written as:

$$v_1 = k_1 \cdot P^{\alpha}_{H_2O}$$

where α is between 0 and 1.

•*Step (II): kinetic of pure diffusion of* O'_{OH} *defects*. According to the first law of Fick, the rate of diffusion is proportional to the gradient of defect concentration $o_+ - o_-$. This leads to:

$$v_2 = k_2.o_+ = k_2 K_1^{1/2} / \left(2K_1^{1/2} + P^{1/2}_{H_2O}\right)$$

In this case, the rate decreases as $P^{-1/2}_{H_2O}$ for high pressures of water vapour and it becomes independent of this pressure at low pressures.

For the other elementary steps, the expressions of the rate of surface area reduction according to the limiting step are summarised in Table 5.

Table 5
Rate expressions of the surface area reduction versus the kinetic constants, the equilibrium constants and the pressure of water vapour according to the possible rate limiting elementary steps

Rate limiting step	Rate
(I)	$v_1 = k_1 \frac{K_4.P_{H_2O}}{\left(2 + K_4^{1/2}.P_{H_2O}^{1/2}\right)^2}$
(II)	$v_2 = k_2 K_1^{1/2} / \left(2K_1^{1/2} + P_{H_2O}^{1/2}\right)$
(III)	$v_3 = \frac{k_3}{\left(2 + K_4^{1/2}.P_{H_2O}^{1/2}\right)^4}$
(IV)	$v_4 = k_4 \frac{K_1.P_{H_2O}}{\left(2K_1^{1/2} + P_{H_2O}^{1/2}\right)^2}$
(V)	$v_5 = k_5 \left(\frac{3}{5}\right)^{5/8} \frac{\left(2K_1^{1/2} + P_{H_2O}^{1/2}\right)^{1/8}}{(K_1 K_7)^{1/16}}$
(VI)	$v_6 = k_6 \left(\frac{K_3}{K_1}\right)^{1/16} \left(\frac{5}{3}\right)^{-3/8} \left(2K_1^{1/2} + P_{H_2O}^{1/2}\right)^{1/8}$
(VII)	$v_7 = k_7.K_3$
(VIII)	$v_8 = k_8.K_s \frac{P_{H_2O}^{1/2}}{2K_1^{1/2} + P_{H_2O}^{1/2}}$

5.2.2. Grain growth by gaseous phase transport

This mechanism is based on the assumption that hydroxyapatite may sublimate without decomposition. The pressure of sublimation depends on the partial pressure of water vapour and the rate of grain growth is proportional to this pressure according to:

$$v_8 = k_8.K_s \frac{P_{H_2O}^{1/2}}{2K_1^{1/2} + P_{H_2O}^{1/2}}$$

In this expression, the kinetic constant k_8 includes the diffusion coefficient by gaseous phase transport. At low pressures of water vapour the rate is proportional to $P_{H_2O}^{1/2}$. It is independent of this pressure for high pressures. For intermediate pressures it can be written as:

$$v_8 = k_8 \cdot P_{H_2O}^{\alpha''}$$

where α'' is between 0 and 0.5.

5.3. Comparison of the experimental results and the model

At 600 °C, the morphological models ($dS/dt = kS^m$) indicate that the rate of surface area reduction is due to superficial diffusion. Moreover, we have demonstrated that the rate of surface reduction was influenced by the pressure of water vapour and was proportional to $P_{H_2O}^{0.68}$. Among the different expressions of the possible limiting rates (Table 5), only the steps (I) and (IV) can be associated with a pressure power law according to a pressure exponent between 0.5 and 1 in a domain of intermediate pressures. These rate laws can be compared with the experimental results through the plots of the inverse of the square root of the rate $v^{-1/2}$ versus the inverse of the square root of the pressure of water vapour$P_{H_2O}^{-1/2}$ for fixed values of the specific surface area. The results are given in Fig. 17. The linear variations of these plots give a good agreement between the model and the experimental data. This confirms that the kinetic of superficial diffusion is controlled by the steps (I) of dehydration and (IV) of hydration that is to say by the adsorption–desorption of water vapour at the surface of the HAP powder. Finally, at 600 °C the theoretical kinetic law of surface area reduction can be expressed as follows:

$$\frac{dS}{dt} = \frac{k_4.K_1.P_{H_2O}}{\left(2K_1^{1/2} + P_{H_2O}^{1/2}\right)^2} \times S^8$$

At 860 °C, the morphological models indicate a matter transport through the gaseous phase. Consequently, we have compared the rate law corresponding to the gaseous mechanism (VIII) with the experimental data. The Fig. 18 shows the plots of the inverse of the rate ($1/v$) versus the inverse of the square root of the pressure of water vapour$P_{H_2O}^{-1/2}$ for fixed values of the specific surface area. The variations are linear and it can be concluded that at 860 °C the theoretical kinetic law of surface area reduction can be written as follows:

$$\frac{dS}{dt} = \frac{k_8.K_s.P_{H_2O}^{1/2}}{\left(2K_1^{1/2} + P_{H_2O}^{1/2}\right)} \times S^6$$

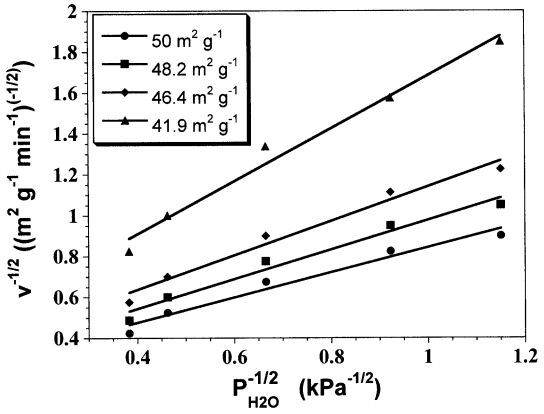

Fig. 17. Relation between $v^{-1/2}$ and $P_{H_2O}^{-1/2}$ of powders calcined at 600 °C for fixed surface areas.

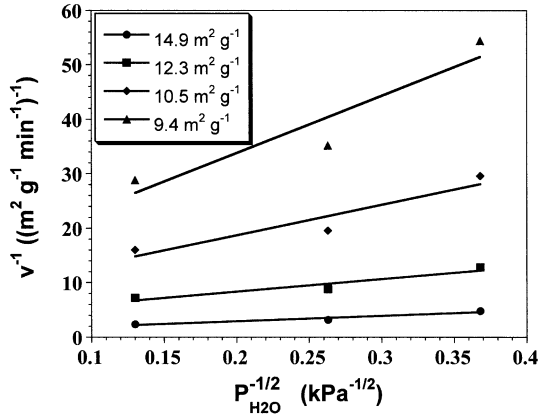

Fig. 18. Relation between v^{-1} and $P_{H_2O}^{-1/2}$ of powders calcined at 860 °C for fixed surface areas.

But, it must be aware of the limits of this model of grain growth based on the hypothesis of grain coalescence in the domain of high temperatures ($T > 850$ °C) because the densification of the material occurs and should become predominant as the temperature increases. Consequently, several additional mechanisms of matter transport (i.e. volume diffusion and/or grain boundary diffusion) that must become preponderant have to be taken in account of.

6. Conclusion

The kinetic laws established in this study allow the separation and the quantification of the respective influences of the gaseous atmosphere and of the grain size. This analysis leads to the conclusion that whatever the temperature might be the water vapour catalyses the grain growth of hydroxyapatite. This result is in agreement with those established for several other ceramic oxides.

The model allows the identification of the elementary processes and the determination of the mechanisms responsible for the surface area reduction during the calcination of HAP powders. Below 850 °C, the superficial diffusion is predominant and the adsorption-desorption of water vapour on the surface of the HAP controls this diffusion. Above 850 °C, temperature at which the densification begins, the surface area reduction could result from gaseous phase transport but also from mechanisms that are effective in the densification of the material (volume diffusion, grain boundary diffusion). The study of these mechanisms will be presented in the second part of this two-part work that will be devoted to the analysis of the densification of the hydroxyapatite either by natural sintering or hot pressing.

References

1. De Groot, K., In *Bioceramics of Calcium Phosphate*, ed. K. De Groot. CRC Press, Boca Raton, FL, 1983, pp. 99–114.
2. Hench, L. L., Bioceramics: from concept to clinic. *J. Am. Ceram. Soc.*, 1991, **74**(7), 1487–1510.
3. Bonel, G., Hydroxyapatite biomaterials: industrial and clinical aspects; evolution of the conceptions. In *Calcium Phosphate Materials Fundamentals*, ed. E. Brès and P. Hardouin. Sauramps Medical, Montpellier, 1998, pp. 9–24.
4. Pontier, C., Viana, M., Champion, E., Bernache-Assollant, D. and Chulia, D., About the use of stoichiometric hydroxyapatite in compression—incidence of manufacturing process on compressibility. *Eur. J. Pharm. Biopharm.*, 2001, **51**, 249–257.
5. Gautier, S., Champion, E. and Bernache-Assollant, D., Processing, microstructure and toughness of Al_2O_3 platelet -reinforced hydroxyapatite. *J. Eur. Ceram. Soc.*, 1997, **17**, 1361–1369.
6. Binner, J. B. P. and Reichert, J., Processing of hydroxyapatite ceramic foams. *J. Mater. Sci.*, 1996, **31**, 5517–5723.
7. Descamps, M., Rin, G., Leger, D. and Thierry, B., Tape-casting: relationship between organic constituents and the physical and mechanical properties of tapes. *J. Eur. Ceram. Soc.*, 1995, **15**, 357–362.
8. Nordström, E. G. and Karlsson, K. H., Slip cast apatite ceramics. *Ceram. Bull.*, 1990, **69**, 824–827.
9. Toriyama, M., Ravaglioli, A., Krajewski, A., Galassi, C., Roncari, E. and Piancastelli, A., Slip casting of mechanochemically synthesized hydroxyapatite. *J. Mater. Sci.*, 1995, **30**, 3216–3221.
10. Santos, J. D., Reis, R. L., Monteiro, F. J., Knowles, J. C. and Hastings, G. W., Liquid phase sintering of hydroxyapatite by phosphate and silicate glass additions: Structure and properties of the composites. *J. Mat. Sci.: Mater. Med.*, 1995, **6**, 348–352.
11. Brossa, F., Cigada, A., Chiesa, R., Paracchini, L. and Consonni, C., Post-deposition treatment effects on hydroxyapatite vacuum plasma spray coatings. *J. Mat. Sci.: Mater. Med.*, 1994, **5**, 855–857.
12. McPherson, R., Gane, N. and Bastow, T. J., Structural characterization of plasma-sprayed hydroxylapatite coatings. *J. Mat. Sci.: Mater. Med.*, 1995, **6**, 327–334.
13. Frayssinet, P., Tourenne, F., Rouquet, N., Conte, P. and Delga, C., Comparative biological properties of HA plasma-sprayed coatings having different crystallinities. *J. Mat. Sci.: Mater. Med.*, 1994, **5**, 11–17.
14. Redey, S., Nardin, M., Bernache-Assollant, D., Rey, C., Delannoy, P., Sedel, L. and Marie, P. J., Behavior of human osteoblastic cells on stoichiometric hydroxyapatite and type A carbonate apatite: role of surface energy. *J. Biomed. Mater. Res.*, 2000, **50**, 353–364.
15. Hott, M., Noel, B., Bernache-Assollant, D., Rey, C. and Marie, P. J., Proliferation and differentiation of human trabecular osteoblasts in long term culture on hydroxyapatite. *J. Biomed. Mater. Res.*, 1997, **37**, 508–516.
16. Raynaud, S., Champion, E. and Bernache-Assollant, D., Calcium phosphate apatites with variable Ca/P atomic ratio, II—calcination and sintering. *Biomaterials*, 2002, **23**, 1073–1080.
17. Barralet, J. E., Best, S. M. and Bonfield, W., Effect of sintering parameters on the density and microstructure of carbonate hydroxyapatite. *J. Mat. Sci.: Mater. Med.*, 2000, **11**, 719–724.
18. Landi, E., Tampieri, A., Celotti, G. and Sprio, S., Densification behaviour and mechanisms of synthetic hydroxyapatites. *J. Eur. Ceram. Soc.*, 2000, **20**, 2377–2387.
19. Jarcho, M., Bolen, C. H., Thomas, M. B., Bobick, J., Kay, F. and Doremus, H., Hydroxylapatite synthesis and characterization in dense polycrystalline form. *J. Mater. Sci.*, 1976, **11**, 2027–2035.
20. Osaka, A., Miura, Y., Takeuchi, K., Asada, M. and Takahashi, K., Calcium apatite prepared from calcium hydroxide and orthophosphoric acid. *J. Mat. Sci.: Mater. Med.*, 1991, **2**, 51–55.

21. Readey, D. W., Lee, J. and Quadir, T., Vapor transport and sintering of ceramics, sintering and heterogeous catalysis. In *Mater. Sci. Monogr.*, ed. G. C. Kuszynski, A. E. Miller and G. A. Sargent. Plenum Press, New York, 1984, pp. 115–136.
22. Hebrard, J., Nortier, P., Pijolat, M. and Soustelle, M., Initial sintering of submicrometer titania anatase powder. *J. Am. Ceram. Soc.*, 1990, **73**(1), 79–84.
23. Pask, J. A., Effect of water vapor on sintering of ceramic oxides. In *Proceedings of the 1st International Symposium on Hydrothermal Reactions*, ed. S. Somiya. Tokyo Institute of Technology, Tokyo, 1983, pp. 904–918.
24. Borgwardt, R. H., Calcium oxide sintering in atmospheres containing water and carbon dioxide. *Ind. Eng. Chem. Res.*, 1989, **28**, 493–500.
25. Anderson, P., Horlock, R. F. and Avery, R. F., Some effects of water vapor during the preparation and calcination of oxide powders. *Proc. Brit. Ceram. Soc.*, 1965, **3**, 33–40.
26. Whittemore, O. J. and Varela, J. R., Initial sintering of MgO in several water vapor pressures. In *Advances in Ceramics 10*. Am. Ceram. Soc., Columbus, 1984, pp. 583–591.
27. Riboud, P. V., Composition et stabilité des phases à structure d'apatite dans le système CaO-P_2O_5-Oxyde de fer-H_2O à haute température. *Ann. Chim. Fr.*, 1973, **8**, 381–390.
28. Raynaud, S., Champion, E., Bernache-Assollant, D. and Laval, J. P., Determination of calcium/phosphorus atomic ratio of calcium phosphate apatites using X-ray diffractometry. *J. Am. Ceram. Soc.*, 2001, **84**(2), 355–366.
29. AFNOR designation NF S 94–066. *Détermination quantitative du Rapport Ca/P de Phosphates de Calcium*. AFNOR, Paris, 1998.
30. German, R. M. and Munir, Z. A., Surface area reduction during isothermal sintering. *J. Am. Ceram. Soc.*, 1976, **59**(9–10), 379–383.
31. German, R. M., Surface area reduction kinetics during intermediate stage sintering. *J. Am. Ceram. Soc.*, 1978, **61**(5–6), 272–274.
32. Ruckenstein, E. and Pulvermacher, B., Kinetics of crystallite sintering during heat treatment of supported metal catalysts. *AIChE. J.*, 1973, **19**, 356–364.
33. Hashimoto, K. and Masuda, T., Change in surface area of silica-alumina catalyst caused by sintering in steam atmosphere. *J. Chem. Eng. Jap.*, 1985, **18**(1), 71–78.
34. Gruy, F., Lois d'évolution de la distribution granulométrique de poudres d'oxydes métalliques calcinées en présence de gaz réactif. *Ann. Chim. Fr.*, 1993, **18**, 69–82.